Predicting ultrafast Dirac transport channel at the one-dimensional interface of the two-dimensional coplanar ZnO/MoS_2 heterostructure

Chunmei Zhang, Yihan Nie, Ting Liao, Liangzhi Kou, and Aijun Du*
School of Chemistry, Physics and Mechanical Engineering, Queensland University of Technology, Gardens Point Campus, Queensland 4001, Brisbane, Australia

(Received 19 July 2018; revised manuscript received 25 October 2018; published 14 January 2019)

The discovery of high-mobility electron gas at the two-dimensional (2D) $LaAlO_3/SrTiO_3$ heterointerface [A. Ohtomo and H. Hwang, Nature (London) **427**, 423 (2004)] has attracted great research interest due to the ballistic transport of spatially confined electrons. When such kind of valence discontinuity extends to the interface of a well-chosen in-planar 2D heterostructure, a one-dimensional (1D) confined interface can be generated. Herein, through first-principles modeling, we demonstrate that Dirac-cone-like bands emerge at the 1D zigzag interface of a ZnO/MoS_2 lateral heterostructure (LHS), creating a highly mobile 1D transport channel with a high Fermi velocity of 4.5×10^5 m/s. The metallic state at the 1D heterointerface is attributed to the polar discontinuity that introduces excess charge carriers. Nontrivial polarization (excess carriers appear at boundaries) results in a large built-in electric field within the ZnO and MoS_2 monolayers. Remarkably, the ultrafast 1D conducting channel is independent of the arrangements of width (m and n) in the $(ZnO)_m(MoS_2)_n$ LHS, which are further illustrated by tight-binding-based orbital and polarization analysis.

DOI: 10.1103/PhysRevB.99.035424

I. INTRODUCTION

Interface engineering has attracted tremendous interest since the discovery that the superconductivity occurs in the interfaces between $LaAlO_3$ and $SrTiO_3$ [1–3]. Subsequently, numerous new and unusual electronic phases at the interfaces have been found [4], especially the conductive channel in the interface of two insulating systems of Al_2O_3/In_2O_3 [5], ZrO_2/In_2O_3 [6], and half-metallic Dirac electronic phase at the interface CrO_2/TiO_2 superlattice [7]. When extending such heterogenous superlattice from three dimensional (3D) to two dimensional (2D), a one-dimensional (1D) interface will be generated and might offer a novel 1D transport channel with potential application in electronics. Importantly, the successful fabrication of varieties of monolayer materials makes the study of 1D interfaces accessible. Some 2D lateral heterostructures (LHS) have been experimentally synthesized [8–12] and some are theoretically predicted [13–15], such as WS_2/MoS_2 [8], WSe_2/MoS_2 [9], Bi_2Se_3/Bi_2Te_3 [12], MoS_2/graphene [16], h-BN/graphene [10,17], and so on [18]. But, works are rather rare compared with the numerous 2D materials. And beyond the graphene participated interface, none of the reported 2D LHS could afford the highly conductive 1D transport channel, which extremely hinders the electronics application. Thus, the current studies of the LHS are still in its infancy and the exploration of more suitable basic building blocks available to create LHS is in high demand.

The monolayer ZnO [19] grown on Ag(111) was fabricated by Tusche and MoS_2 [20] grown on silicon substrate was synthesized in experiments; both are wide-band-gap semiconductors. So far, some fantastic features have been detected on the MoS_2/ZnO heterojunctions [21,22], such as the strong photoresponse [23] and good conductivity [21], but mainly focused on the vertically stacked heterostructures. The lateral heterointerface between ZnO and MoS_2 is accessible for experimental realization since their lattices are well matched to one another (3.28 and 3.24 Å, respectively). It should be noted that both 2D ZnO and MoS_2 possess nontrivial polarized properties (excess carriers appear at certain boundaries) [24], and the formed MoS_2/ZnO LHS would result in the excess surface charge along the boundary of the zigzag nanoribbon, while it would vanish for armchair directions. Therefore, fascinating electronic and physical properties are expected to be presented at the 1D interface of MoS_2/ZnO LHS.

In this work, based on first-principles modeling, we propose a 2D ZnO/MoS_2 LHS with a lower formation energy than that of a fabricated graphene/h-BN 2D superlattice [25]. A Dirac cone emerges at the 1D zigzag interfaces of the ZnO/MoS_2 LHS with an ultrahigh Fermi velocity (4.5×10^5 m/s) which is comparable to that of graphene. Since ZnO and MoS_2 monolayers harbor nontrivial polarization properties, the polar discontinuity introduces free carriers at two interfaces, which accounts for the ultrafast transport channel. The generated net charges with opposite signs at two interfaces then introduce building an electric field inside the ZnO and MoS_2 bulk. The polarized carriers are not affected by the length of the nanoribbon, and therefore the 1D ultrafast transport channel along the zigzag direction remains while tuning the different ratios of the ZnO and MoS_2 building blocks. This has also been further proven by the tight-binding (TB) method, which was constructed based on the d orbitals of the interfacial Mo atoms.

II. METHODS

All of the calculations were performed using density functional theory (DFT) within the generalized gradient

*Corresponding author: aijun.du@qut.edu.au

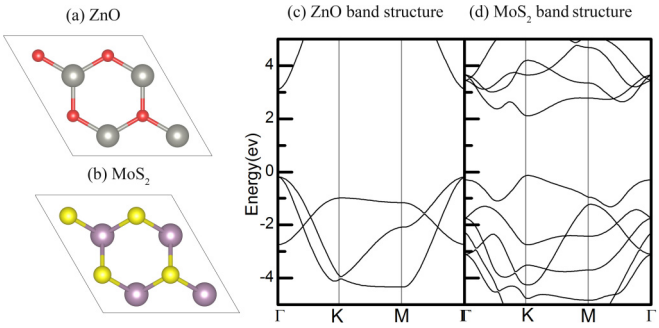

FIG. 1. (a),(b) Top views of structure and (c),(d) band structures of ZnO and MoS_2 monolayers.

approximation of the Perdew-Burke-Ernzerhof (PBE) functional, as implemented in the Vienna *ab initio* simulation package (VASP) [26–28]. The hybrid functional method based on the Heyd-Scuseria-Ernzerhof (HSE) [29] model was adopted to accurately calculate the band structure. A dispersion correction of total energy (DFT-D3 method) [30] was used to incorporate the long-range van der Waals (vdW) interaction. To study 2D systems under the periodic boundary condition, a vacuum layer with a thickness 18 Å and a plane-wave basis set with an energy cutoff of 500 eV was set to minimize artificial interactions between neighboring layers. The structures studied here were fully relaxed until energy and force converged to 10^{-6} eV and 0.001 eV/Å, respectively. The band structures of 2D ZnO/MoS_2 LHS were calculated with Monkhorst k-point meshes of 0.0015 $Å^{-1}$. In addition, the spin-orbital coupling (SOC) is considered in this calculation.

III. RESULTS AND DISCUSSION

In monolayer ZnO, the Zn and O atoms are arranged in a hexagonal honeycomb lattice as shown in Fig. 1(a). The monolayer 2H phase MoS_2 is composed of two hexagonal planes of S atoms and a hexagonal plane of M atoms sandwiched in between [Fig. 1(b)]. The monolayer structures of MoS_2 [31] and ZnO [19] have been fabricated in experiments and their band gaps are calculated to be 2.24 [Fig. 1(d)] and 3.29 eV [Fig. 1(c)], respectively, which are in good agreement with previous work [32,33].

The lattice mismatch between the MoS_2 and ZnO monolayer is less than 1%, indicating a low formation energy of 2D LHS. Here we considered the interfacial atomic configurations of MoS_2/ZnO with zigzag [Fig. 2(a)] and armchair-type interface, which is presented in Fig. S1(a) of the Supplemental Material [34]. The energies of the LHS can be calculated by using 2D MoS_2 and ZnO monolayer as a reference. We define the formation energy as [25]

$$E_{\text{form}} = (E_{\text{LHS}} - n_{\text{MoS}_2} E_{\text{MoS}_2} - n_{\text{ZnO}} E_{\text{ZnO}})/2l, \qquad (1)$$

where E_{LHS}, E_{ZnO} (E_{MoS_2}), n_{ZnO} (n_{MoS_2}), and l are the total energy of the LHS, the total energies of a primitive cell of ZnO (MoS_2), the number of Zn-O(Mo-S_2) pairs, and the periodic length along the zigzag/armchair interface, respectively. The 1/2 coefficient represents two interfaces within a unit cell. The bonding energy of an interface is defined as the energy needed to cleave the geometry along the interface without

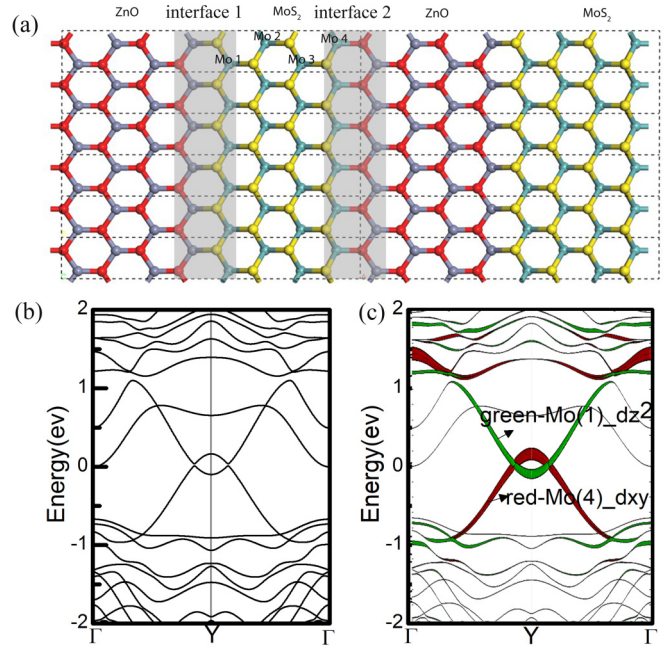

FIG. 2. (a) The lattice structures, (b) band structures, and (c) orbital-resolved band structure of periodic $(ZnO)_4(MoS_2)_4$ LHS along the zigzag direction. Zn, O, Mo, and S are marked by red, gray, cyan, and yellow, respectively. The Fermi level is shifted into energy 0 eV in (b) and (c).

relaxation. Figure 2(a) illustrates the typical lattice structures of periodic LHS. For simplification, the ZnO/MoS_2 monolayer LHS is denoted as $(ZnO)_m(MoS_2)_n$ LHS, where the indexes of m and n indicate the number of different building blocks [Fig. 2(a)]. The formation energies for zigzag and armchair interface of $(ZnO)_4(MoS_2)_4$ LHS [Fig. 2(a)] are 2.12 eV/nm and 2.25 eV/nm, respectively, which are even lower than that of already fabricated graphene/h-BN in-plane LHS (∼2.2–2.9 eV/nm) [17,25]. The smaller the m and n values, the lower the formation energy is. To avoid the interactions between interfaces, a sufficiently large supercell is used, in which the width (armchair direction) is up to 23 Å in the $(ZnO)_4(MoS_2)_4$ LHS. The periodic boundary conditions for zigzag $(ZnO)_4(MoS_2)_4$ LHS result in two types of 1D heterointerfaces, Zn-S and Mo-O interface.

The band structures of $(ZnO)_4(MoS_2)_4$ LHS along the zigzag and armchair interfaces are then calculated as shown in Fig. 2(b) and Fig. S1(b) of the Supplemental Material [34]. The band gaps are 0 and 0.694 eV, respectively, for the zigzag and armchair interfaces of $(ZnO)_4(MoS_2)_4$ LHS by the PBE method, which are totally different from that of the pristine MoS_2 and ZnO monolayers shown in Figs. 1(c) and 1(d). As we can see in Fig. 2(b), a Dirac cone emerges along the Γ–Y line (zigzag direction). Around the Dirac cone, the valence and conduction bands exhibit a linear dispersion across the Fermi level, indicating that charge carriers (electrons and holes) in these bands behave as a small mass of Dirac fermions [35–38]. The Fermi velocity is $v_f = 4.5 \times 10^5$ m/s, which is comparable to that of graphene (1.1×10^6 m/s) [39]. Thus, the extremely high carrier mobility can be obtained at the 1D interfaces. The hybrid density functional (HSE06) calculation was also employed to double check that the Dirac cone is

still robust in the electronic band structures (Fig. S2 in the Supplemental Material [34]). When the SOC effect is incorporated, the Dirac cone is still located around the Y point with a slight band splitting for $(ZnO)_4(MoS_2)_4$ LHS along the zigzag interface, as shown in Fig. S3 (Supplemental Material [34]).

To explore the origin of the Dirac cone, we calculated the orbital resolved band structures [Fig. 2(c)]. It can be clearly seen from Fig. 2(c) that the states of the Dirac cone in $(ZnO)_4(MoS_2)_4$ LHS are dominated by the d orbitals from interface Mo atoms: d_{z2} orbitals of Mo1 atoms and d_{xy} orbitals of Mo4 atoms. Thus, the two interfaces are n (interface 1) and p type (interface 2), respectively. Similarly, this can be further confirmed by the projected density of states (PDOS) and spatial charge analysis of the $(ZnO)_4(MoS_2)_4$ LHS (which are shown in Figs. S4 and S5 of the Supplemental Material [34]). Most interestingly, there is a band inversion between the valence-band (VB) and conduction-band (CB) edges around the Y point, as shown in Fig 2(c).

As the valence and conduction bands for the Dirac cone of $(ZnO)_4(MoS_2)_4$ LHS are mainly contributed by the hybridization of d_{xy} of Mo 4 and d_{z^2} orbitals of Mo 1 atoms, we can construct a two-band effective TB model along the Γ1-Y (between the line Γ-Y) line on the basis of d_{xy} and d_{z^2} of Mo atoms (see Supplemental Material [34] for more details on the TB method). The Hamiltonian can be written as

$$H = \begin{bmatrix} \varepsilon_1 & tf(k) \\ tf^*(k) & \varepsilon_2 \end{bmatrix},$$

$$H_{Mo\_4\_dxy\,Mo\_4\_dxy} = \varepsilon_1,$$

$$H_{Mo\_1\_d_{z^2}\,Mo\_1\_d_{z^2}} = \varepsilon_2,$$

$$f\ (k) = i * \sin(0.5 * b * ky).$$

Here, ε_1 and ε_2 denote the on-site energy for the d_{xy} orbital of Mo 4 atoms and the d_{z^2} orbitals of Mo 1 atoms, and t is the hopping parameter between the d_{xy} orbital of Mo4 and d_{z^2} orbital of Mo 1 atoms along the ky direction. As the $f(k)$ equation is determined by the ky parameter, only hopping along the y direction matters. By fitting with the DFT results, we get the corresponding on-site energy and hopping parameters: $t = -0.6$ eV, $\varepsilon_1 = -0.02$ eV, $\varepsilon_2 = -0.02$ eV. Our TB results are in good agreement with the first-principles results (Fig. 3). The hopping parameter t determines the amplitude of the conduction-band minimum (CBM) and valence-band maximum (VBM), while the ε_1, ε_2 controls that the Dirac cone is located at the Fermi surface. Based on this, the Dirac cone is only determined by the on-site energy and the hopping parameter t along the y direction. Thus the changing of the different ratios of building blocks (ZnO and MoS_2) in $(ZnO)_m(MoS_2)_n$ LHS barely affects the band structure and the Dirac cone, as they only alter the length between the Mo1 and Mo4 atoms along the x direction. Our further DFT calculations confirmed that the Dirac cones are completely unaffected in the band structure of $(ZnO)_4(MoS_2)_4$, $(ZnO)_6(MoS_2)_6$, $(ZnO)_8(MoS_2)_8$, $(ZnO)_{10}(MoS_2)_{10}$, $(ZnO)_4(MoS_2)_8$, and $(ZnO)_8(MoS_2)_4$ LHS, which are shown in Fig. S6 of the Supplemental Material [34], which agree with our anticipation.

Normally charge transfer accounts for the conductivity at the two interfaces of the insulator [40]. However, there is no significant charge transfer between the ZnO and MoS_2 monolayers based on our Bader charge analysis. Then the question becomes why could the ultrafast channel be created in the interface of two semiconducting materials? Both monolayer ZnO and MoS_2 are charge-neutral nanosheets, and the valence states can be assigned as Zn^{2+}, O^{2-}, Mo^{4+}, and S^{2-}. Polar discontinuities can be generated in the two interfaces of 2D ZnO/MoS_2 LHS. According to the formal polarization theory [24], the built-in polarity discontinuity of the interfaces in the $(ZnO)_4(MoS_2)_4$ LHS introduces the polarization carriers.

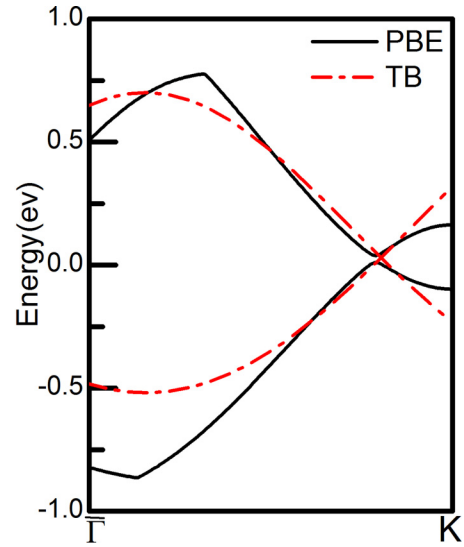

FIG. 3. The calculated band structure for $(ZnO)_4(MoS_2)_4$ LHS by the PBE method (black line) and TB method (red dashed line).

The contribution of an electron to the electric polarization can be represented by a point charge $-e$ located at the center of the corresponding Wannier function constructed from all the occupied Bloch states. Suppose that the unit cell of the ZnO [Fig. 4(a)] and MoS_2 [Fig. 4(b)] contains ions located at positions r_α with charges Q_α (the index α labels ions), and the Wannier functions of electrons are centered at r_i (the index i labels electrons) [41]. The polarization in the area of the unit cell S is then described as follows [41]:

$$P = \frac{1}{S}\sum_\alpha Q_\alpha r_\alpha - e\sum_i r_i\ . \tag{2}$$

Here, the Q for Zn, O, Mo, and S atoms are $+2e$, $+6e$, $+4e$, and $+6e$, respectively. For the primitive unit cell of ZnO, one cation (Zn) and one anion (O) are included [41], while for MoS_2, for convenience, a rectangular unit containing two cations (Mo) and four anions (S) is adopted [the blue shade in Fig. 4(a)] [42]. Considering the spin degeneracy, each Wannier function represents a point charge of $-2e$ at its center. For the primitive cell of ZnO, one of the Wannier functions has its center located at the anion (O) site; the other three are located on the three anion-cation (O-Zn) bonds with a shorter distance to the O ion [13]. When it comes to MoS_2, six p-like doubly degenerate Wannier functions are located around the S ions, while another transition-metal d orbital is located in the middle of the hexagonal cell [42]. Thus we get the bulk formal polarization for ZnO and MoS_2 monolayers along x

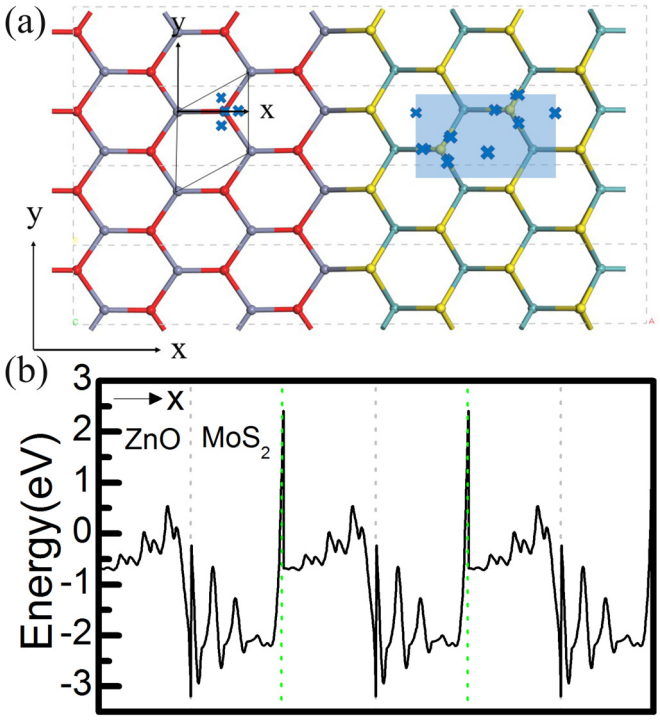

FIG. 4. (a) Centers of Wannier functions are represented by crosses in the ZnO and MoS_2 unit cell. In ZnO, the upper valence bands can be mapped into four doubly degenerate Wannier functions centered around the anion (red balls). In the Wannier function centers for MoS_2, six doubly degenerate Wannier functions are located around the chalcogens (yellow balls), while another one is located in the middle of the hexagonal cell. The gray, red, yellow, and blue balls represent Zn, O, S, and Mo atoms respectively. (b) Average of 2D electrostatic potential difference between 2D $(ZnO)_4(MoS_2)_4$ LHS along the x axis. The gray and green dots denote the positions of interface 1 and interface 2, respectively. Three repeated periods are presented.

directions (normal to the 1D interface), $P_x^{(MoS_2)} = P_x^{(ZnO)} = \frac{2e}{3a}$, where a is the relaxed lattice parameter in $(ZnO)_4(MoS_2)_4$ LHS, "+" denotes the cation (Zn, Mo) terminated edges, and "−" presents the anion (O, S) terminated edges. The polar discontinuity is corresponding to a bound interface charge. For the 1D zigzag interface between 2D ZnO and MoS_2, the line density of bound charge λ_{bound} [41] is then equal to the discontinuity of the component of the polarization normal to the interface direction,

$$\lambda_{bound} = P_x^{(MoS_2)} - P_x^{(ZnO)}. \quad (3)$$

From Eq. (3), we can infer that polarized electrons and holes could be generated at the heterointerfaces 1 and 2, with λ being approximately $-\frac{4e}{3a}$ and $+\frac{4e}{3a}$, respectively. Also, the interface carriers are not affected by the length of the ribbon along x, which is consistent with the conclusion reached by our tight-binding theory analysis that the Dirac cone keeps intact while assigning the different values of m and n in the $(ZnO)_m(MoS_2)_n$ LHS. However, the polarization carriers will vanish along the armchair direction for the ZnO and MoS_2 monolayer and $P_y^{(MoS_2)} = P_y^{(ZnO)} = 0$. Thus, no current can be observed that crosses the Fermi surface along the armchair direction of $(ZnO)_m(MoS_2)_n$ LHS, as shown in Figs. S2 and S7 of the Supplemental Material [34].

In the zigzag interface of the $(ZnO)_4(MoS_2)_4$ LHS, the net charges at the interfaces would give rise to an intrinsic electric field inside the MoS_2 and ZnO regions. We further calculated the effective electrostatic potential difference in LHS by subtracting the total potential of single-layer MoS_2 and MoS_2 from that of 2D $(ZnO)_4(MoS_2)_4$ LHS, and then taking an average in the plane along the x axis, as shown in Fig. 4(b). The electric potential difference of the LHS exhibited a repeated sawtoothlike profile along the x axis, indicating an electric field of opposite polarity. The electrical potential increases/decreases inside ZnO/MoS_2 and this is consistent with the previous analysis from the modern theory of polarization that negative and positive polarized net carriers accumulated at interface 1 and 2, respectively. The abrupt steplike transition at the zigzag interface of $(ZnO)_4(MoS_2)_4$ LHS indicates the accumulation of net carriers. The band inversion shown in Fig. 2(c) may be due to the built-in electric field as demonstrated in the vertical heterojunctions [43].

IV. CONCLUSIONS

In conclusion, based on the first-principles theory, we have investigated the electronic structure of the 1D interface of the $(ZnO)_m(MoS_2)_n$ LHS. The 1D highly conductive channel (Dirac cone) emerges at the zigzag interface, while a big band gap opened at the armchair interface of the $(ZnO)_m(MoS_2)_n$ LHS. The VBM at the p-type (Mo-O) interface and the CBM at the n-type (Zn-S) interface are contributed by the d orbitals of the interfacial Mo atoms. The TB theory demonstrates that the Dirac cone along the zigzag interface can keep intact, irrelevant with respect to the m and n values in $(ZnO)_m(MoS_2)_n$ LHS, which is further proved by the polarization theory. In addition, since a modified step-by-step thermal CVD process has been designed to form the reliable monolayer LHS [44] and many lateral p-n junctions have been synthesized despite a large lattice mismatch. Thus, the little lattice mismatch and low formation energy make sure that the high-quality lateral connections can be formed in $(ZnO)_m(MoS_2)_n$ LHS. Moreover, we find that monolayer GaN can be a proper substrate [45] to integrate ZnO/MoS_2 LHS (see Fig. S8 of the Supplemental Material [34]). Besides, monolayers ZnO and MoS_2 can be replaced by other fabricated 2D materials sharing the same structure with them, such as monolayers GaN [46], AlN [47] and $MoSe_2$ [48], WS_2 [49]. Similar results have been achieved in GaN/MoS_2, AlN/MoS_2, $ZnO/MoSe_2$, and ZnO/WS_2 LHS, shown in Fig. S9 of the Supplemental Material [34]. These findings suggest that LHS formed by MoS_2- and ZnO-type structures are a promising material for the next-generation all-2D circuitry with extraordinary electrical performance.

ACKNOWLEDGMENTS

A.D. acknowledges the financial support by the Australian Research Council under the Discovery Project (No. DP170103598) and also the computer resources provided through high-performance computer time at the computing facility at the Queensland University of Technology,

NCI National Facility, and The Pawsey Supercomputing Centre through the National Computational Merit Allocation Scheme supported by the Australian Government and the Government of Western Australia.

[1] G. Herranz *et al.*, Phys. Rev. Lett. **98**, 216803 (2007).
[2] X. Wang *et al.*, Nat. Commun. **2**, 188 (2011).
[3] A. Ohtomo and H. Hwang, Nature (London) **427**, 423 (2004).
[4] A. Du, Wiley Interdiscip. Rev. Comput. Mol. Sci. **6**, 551 (2016).
[5] S. Y. Lee, J. Kim, A. Park, J. Park, and H. Seo, ACS Nano **11**, 6040 (2017).
[6] K. Zhang *et al.*, Chem. Mater. **21**, 4353 (2009).
[7] T. Cai, X. Li, F. Wang, S. Ju, J. Feng, and C.-D. Gong, Nano Lett. **15**, 6434 (2015).
[8] C. Huang *et al.*, Nat. Mater. **13**, 1096 (2014).
[9] M.-Y. Li *et al.*, Science **349**, 524 (2015).
[10] M. Liu *et al.*, Nano Lett. **14**, 6342 (2014).
[11] H. Li, P. Li, J.-K. Huang, M.-Y. Li, C.-W. Yang, Y. Shi, X.-X. Zhang, and L.-J. Li, ACS Nano **10**, 10516 (2016).
[12] S. Lou *et al.*, Nano Lett. **18**, 1819 (2018).
[13] G.-X. Chen, X.-G. Li, Y.-P. Wang, J. N. Fry, and H.-P. Cheng, Phys. Rev. B **95**, 045302 (2017).
[14] N. C. Bristowe, M. Stengel, P. B. Littlewood, E. Artacho, and J. M. Pruneda, Phys. Rev. B **88**, 161411(R) (2013).
[15] J. M. Pruneda, Phys. Rev. B **81**, 161409(R) (2010).
[16] A. Behranginia *et al.*, Small **13**, 1604301 (2017).
[17] L. Ci *et al.*, Nat. Mater. **9**, 430 (2010).
[18] X.-L. Wang, S. X. Dou, and C. Zhang, NPG Asia Mater. **2**, 31 (2010).
[19] C. Tusche, H. L. Meyerheim, and J. Kirschner, Phys. Rev. Lett. **99**, 026102 (2007).
[20] S. Helveg, J. V. Lauritsen, E. Lægsgaard, I. Stensgaard, J. K. Nørskov, B. S. Clausen, H. Topsøe, and F. Besenbacher, Phys. Rev. Lett. **84**, 951 (2000).
[21] P. Liang, B. Tai, H. Shu, T. Shen, and Q. Dong, Solid State Commun. **204**, 67 (2015).
[22] L. Chen, F. Xue, X. Li, X. Huang, L. Wang, J. Kou, and Z. L. Wang, ACS Nano **10**, 1546 (2015).
[23] F. Xue *et al.*, Adv. Mater. **28**, 3391 (2016).
[24] D. Vanderbilt and R. D. King-Smith, Phys. Rev. B **48**, 4442 (1993).
[25] J. Zhang, W. Xie, X. Xu, S. Zhang, and J. Zhao, Chem. Mater. **28**, 5022 (2016).
[26] G. Kresse and J. Hafner, Phys. Rev. B **47**, 558 (1993).
[27] G. Kresse and J. Furthmüller, Phys. Rev. B **54**, 11169 (1996).
[28] P. E. Blöchl, Phys. Rev. B **50**, 17953 (1994).
[29] J. Heyd, G. E. Scuseria, and M. Ernzerhof, J. Chem. Phys. **118**, 8207 (2003).
[30] S. Grimme, J. Comput. Chem. **27**, 1787 (2006).
[31] J. Zheng, H. Zhang, S. Dong, Y. Liu, C. T. Nai, H. S. Shin, H. Y. Jeong, B. Liu, and K. P. Loh, Nat. Commun. **5**, 2995 (2014).
[32] K. F. Mak, C. Lee, J. Hone, J. Shan, and T. F. Heinz, Phys. Rev. Lett. **105**, 136805 (2010).
[33] M. Topsakal, S. Cahangirov, E. Bekaroglu, and S. Ciraci, Phys. Rev. B **80**, 235119 (2009).
[34] See Supplemental Material at http://link.aps.org/supplemental/10.1103/PhysRevB.99.035424 for band structures along the armchair and zigzag directions by PBE, HSE, and TB methods, the PDOS, spatial charge distribution of CBM and VBM, band structures of different ratios of MoS_2 and ZnO building blocks, ZnO/MoS_2 LHS growth on substrate, as well as other 2D superlattices composed of ZnO- and MoS_2-like monolayers.
[35] C. Zhang, Y. Jiao, L. Kou, T. Liao, and A. Du, J. Mater. Chem. C **6**, 6132, (2018).
[36] Y. Jiao, F. Ma, C. Zhang, J. Bell, S. Sanvito, and A. Du, Phys. Rev. Lett. **119**, 016403 (2017).
[37] C. Zhang and A. Du, Beilstein J. Nanotechnol. **9**, 1399 (2018).
[38] C. Zhang, Y. Jiao, F. Ma, S. Bottle, M. Zhao, Z. Chen, and A. Du, Phys. Chem. Phys. Chem. **19**, 5449 (2017).
[39] P. E. Trevisanutto, C. Giorgetti, L. Reining, M. Ladisa, and V. Olevano, Phys. Rev. Lett. **101**, 226405 (2008).
[40] Y. Liu, Y.-L. Zhu, Y.-L. Tang, Y.-J. Wang, Y.-X. Jiang, Y.-B. Xu, B. Zhang, and X.-L. Ma, Nano Lett. **17**, 3619 (2017).
[41] M. Gibertini, G. Pizzi, and N. Marzari, Nat. Commun. **5**, 5157 (2014).
[42] M. Gibertini and N. Marzari, Nano Lett. **15**, 6229 (2015).
[43] C. Zhang, Y. Jiao, T. He, S. Bottle, T. Frauenheim, and A. Du, J. Phys. Chem. Lett. **9**, 858 (2018).
[44] Z. Zhang, P. Chen, X. Duan, K. Zang, J. Luo, and X. Duan, Science **357**, 788 (2017).
[45] J. Zeng, P. Cui, and Z. Zhang, Phys. Rev. Lett. **118**, 046101 (2017).
[46] Z. Y. Al Balushi *et al.*, Nat. Mater. **15**, 1166 (2016).
[47] P. Tsipas *et al.*, Appl. Phys. Lett. **103**, 251605 (2013).
[48] M. M. Ugeda *et al.*, Nat. Mater. **13**, 1091 (2014).
[49] H. M. Hill, A. F. Rigosi, C. Roquelet, A. Chernikov, T. C. Berkelbach, D. R. Reichman, M. S. Hybertsen, L. E. Brus, and T. F. Heinz, Nano Lett. **15**, 2992 (2015).